Solvent and Intermolecular Effects on First Hyperpolarizabilities of Organometallic Tungsten−Carbonyl Complexes, A TDDFT Study

Qiaohong Li, Rongjian Sa, Caiping Liu, and Kechen Wu*

State Key Laboratory of Structural Chemistry, Fujian Institute of Research on the Structure of Matter, Chinese Academy of Sciences, Fuzhou 350002, People's Republic of China

Received: March 29, 2007; In Final Form: June 26, 2007

The first hyperpolarizability of two tungsten−carbonyl complexes, tungsten pentacarbonyl pyridine and tungsten pentacarbonyl *trans*-1,2-bis(4-pyridyl)-ethylene, has been studied by the high-level TDDFT method. The consideration of the solvent effect and intermolecular $\pi-\pi$ weak interaction in the calculations quantitatively improve the final result of both the electronic excitations and the first hyperpolarizabilities. By using the orbital decomposition scheme (*J. Phys. Chem. A* **2006**, *110*, 1014−1021), the NLO mechanisms of these two complexes have been ascribed to the dominant contribution from the metal-to-ligand charge transfer, with HOMO → LUMO character, and the indispensable contribution from the intraligand charge transfer as well. A supplementary formula has been proposed to implement the orbital-pair transition analysis. This study reports the significant influences of solvation and intermolecular interactions on the first hyperpolarizabilities of organometallic NLO chromophores.

1. Introduction

Organometallic and metal cluster coordination complexes have been attracting great interest in recent years as the effective nonlinear optical (NLO) materials/chromophores because they combine the superior characteristics of organic and inorganic materials.[1,2] The existence of transition metal (TM) atom and extended conjugate π-delocalization ligands sufficiently provide the push−pull architecture in such a chromophore that is necessary for the significant hyperpolarizability.[3]

The elucidations of the NLO mechanism of organometallic and metal cluster complexes are important in the development of novel TM NLO chromophores. The available experimental measurements reported so far are limited on the first hyperpolarizabilities (β) of organometallic chromophores. Some of them have indicated the critical role of the metal-to-ligand charge transfer (MLCT) mechanism.[4,5] It would be more complicated than the polynuclear metal cluster complexes with metal−metal bonds, and less reports on the topic are available so far.[6] One of the pathways to effectively understand the NLO mechanism of such a metal cluster coordination complex is to put the basis on the understanding of that of the organometallic complexes containing only one TM atom.

The metal−carbonyl complex is one of the mostly investigated organometallic complexes. Among the hundreds of synthesized metal−carbonyl complexes, there are some that have been reported to possess notable second-order NLO responsibilities.[7,8] The aromatic metal−carbonyl complexes with the metal−π binding possess extensive MLCT pattern of charge transfer, which benefits the large β as mentioned above. Cheng et al. reported the measurements of the first hyperpolarizabilities of a series of metal−carbonyl complexes.[9] They showed that the substitute of the arene ligands was an effective way to alter the β and in some cases could change two to three times in the magnitude of β values.

Although many theoretical investigations have been performed on the electronic mechanism of organometallic NLO-phores, the reported first-principles studies are limited so far.[10,11] The recent TDDFT study by Baerends et al. gave an insight into understanding a new effective analysis scheme on the NLO mechanism of a sesquifulvalene transition metal complex.[12] The series studies by Bruschi et al. applied both the ab initio/CIS−SOS and TDDFT/CDDFT methods in particular on the electronic excitations and the β of a series of metal−carbonyl complexes with different π-delocalized ligands, namely Py, PyCHO, Pyz, $PyzBF_3$, BPE, and $BPEBF_3$.[13] The later study led to the interesting conclusions that the DFT results on the first hyperpolarizability of the metal−carbonyl complexes seriously overestimated the experimental, especially for those with extended π-delocalization coordination ligands (BPE and $BPEBF_3$). They pointed out as well the oversimplification of the "two-level model" (TLM) by Oudar.[14]

There are in fact many factors that affect the final calculated results of the β values and the consequent conclusions drawn by the calculations.[15,16] The previous studies have already showed the limitations of the DFT method in the accurate description of the β of organic long molecules basically due to the exchange-correlation (XC) functional approximation.[17] The effects of basis set and methods have been discussed as well. Beside these, there are other limitations of the above theoretical investigations on the organometallic−carbonyl complexes. They lacked in the considerations of the environment effects, for example, the solvation and intermolecular interactions that in some cases are critical in obtaining quantitatively satisfactory results of both the electronic excitations and the β in comparison with the experimental results. To our best knowledge, the reported DFT studies are very limited that take into account both the solvent effect and intermolecular interaction effect on the β of organometallic NLO-phores.

In this paper, we applied TDDFT method at a high level of accuracy to study the first hyperpolarizability of two typical extended π-delocalization tungsten−carbonyl complexes with

* Corresponding author. E-mail: wkc@fjirsm.ac.cn. Telephone: +86-591-93792600. Fax: +86-591-83792932.

10.1021/jp072484s CCC: $37.00
Published on Web 07/26/2007

the considerations of both the solvent effects and intermolecular interactions. We showed that, by such additional considerations, the TDDFT results of β could be significantly improved and therefore comparable in quantity with the measured data. The orbital decomposition scheme proposed by Baerends et al.[12] is useful and effective in analysis the electronic NLO mechanism of the two organometallic chromophores in terms of the simulated electronic excitation transitions.

The paper is organized as follows. In Section 2, we introduce the computational method in detail in the study as well as the modified orbital decomposition scheme in the analysis. In Section 3, two typical organometallic tungsten−carbonyl complexes, $W(CO)_5Py$ (tungsten pentacarbonyl pyridine, TPCP) and $W(CO)_5BPE$ (tungsten pentacarbonyl *trans*-1,2-bis(4-pyridyl)-ethylene (BPE), TPCB), with extended π-delocalization ligands (Py and BPE), are studied and analyzed on both the electronic excitations and first hyperpolarizability. A supermolecular approach has been adopted to account the intermolecular interactions. Two models are used for comparative purposes for both TPCP and TPCB, i.e., the monomer model with and without solvent effects and the dimer model with solvent effect. The former shows the effects of solvation and, in the latter case, both the solvent effect and intermolecular interactions are taken into account. In Section 4, we give our conclusions based on the calculations and electronic mechanism analysis.

2. Computational Methods

The experimental measurements[9] of the dipole moments and the first hyperpolarizability of both TPCP and TPCB complexes were performed by using solution-phase DC electric-field-induced second-harmonic generation (EFISH). TPCP was measured in toluene solution, while TPCB was in chloroform, and both at 1.91 μm incident laser radiation. The volume of solvent molecule in solution, solvent dispersion, solvent dielectric constant, and even the NLO susceptibility of such solution exert influences on the final EFISH measurements. To reduce the discrepancy between the gas-phase calculation and the solution-phase measurement, the solvent effects were employed in this study by using a conductor-like screening model (COSMO)[18] of solvation with the Klamt surface.[19] The solute dielectric constant were set to 2.38 (toluene) and 4.8 (chloroform) for TPCP and TPCB, respectively.

Although the EFISH measurements were performed in dilute solution, the intermolecular interaction is stronger than that in the gas phase. To simulate the interaction effect even within the weak interaction regime in solution-phase EFISH measurement, the supermolecular approach is employed in both TPCP and TPCB dimer models.

The initial geometric structures of TPCP and TPCB chromophores were taken from the X-ray diffraction data.[20,21] The molecular geometries have been fully optimized in the solutions to the local energy minima, which have been confirmed by no imaginary harmonic vibration frequency. All the geometries are in C_1 point group symmetry, except the monomer of TPCP is restricted to C_2 symmetry with the 2-fold axis (y) along the dipole moment direction. The main structural parameters of the monomers of TPCP and TPCB are listed in Table 1. The dimer models of both TPCP and TPCB are fully optimized to such configurations that the interaction energies (ΔE_i) meet the following conditions:

$$\Delta E_i = E_{dimer} - 2E_{monomer} < 0 \qquad (1)$$

TABLE 1: Major Optimized Geometric Parameters (Bond Lengths in Å and Angles in deg) of TPCP and TPCB Monomers

	TPCP	TPCB
W−N	2.244	2.289
$W-C_1$	1.988	2.014
$W-C_{2-5}$	2.033	2.055−2.061
$\angle N-W-C_1$	180.0	180.0
C_6-C_7		1.466
C_7-C_8		1.362
C_8-C_9		1.471

Figure 1 shows the optimized structures of the monomers and dimers. The dimer configurations for TPCP and TPCB could have many possibilities such as head-to-end configuration and head-to-head configuration, etc. However, we found the dimer configurations displayed in Figure 1 met the above interaction energy conditions: ΔE_i(TPCP) was −1.03 eV, while ΔE_i-(TPCB) was −1.3 eV. The basis set superposition error (BSSE) has been examined by the counterpoise method. The BSSE corrections of TPCP and TPCB were all less than 0.01 eV, which was negligible. The intramolecular bond length distortions in the dimer models were all less than 2% versus those in the monomers for both TPCP and TPCB. The W−W distances are 7.38 and 18.77 Å for TPCP and TPCB, respectively.

The geometric optimizations and ground-state self-consistent field (SCF) calculations were proceeded at the TZP Slater basis set with the "small" frozen core level (C, O; 1s; W: 1s4d) by using the XC functional based on the local density approximation (LDA)[22] and the general gradient approximation (GGA) proposed by Beck and Perdew[23] with scalar ZORA approach[24] for relativistic effect, i.e., at the BP/TZP/ZORA level. The SCF procedure was converged to 10^{-8} au and the integration accuracy parameter was set to 5.

The measured excitation data[9,10] of both TPCP and TPCB complexes were obtained in solutions. TPCB's excitation data were measured in benzene, while TPCP's were measured in toluene, so the calculations of electronic excitation spectra of both the monomers and dimers of TPCP and TPCB chromophores were carried out in solution as well. The solvent dielectric constant for benzene was set to 2.25. The calculated spectra with solvent effect could impact the excitations not only in energies but in the intensities.

The RESPONSE module[25] implemented in the Amsterdam density functional program (ADF)[26] has been adopted in the analytical TDDFT calculations of the electronic excitations and the frequency-dependent first hyperpolarizabilities. The XC functions based on the gradient-regulated connection (GRAC)[27] of the potentials based on the shape-corrected LB94 potential proposed by van Leeuwen and Baerends[28] with scalar ZORA approach have been used at the TZ2P Slater basis set with small frozen core level of accuracy. The definition of β_i and β_{vec} is as follows:

$$\beta_{vec} = \sum_{i=x,y,z} \mu_i\beta_i/|\mu|$$

$$\beta_i = \frac{1}{5}\sum_{j=x,y,z}(\beta_{ijj} + \beta_{jij} + \beta_{jji}), \qquad i = x,y,z \qquad (2)$$

The widely used TLM takes into account a particular excitation in analyzing the contribution to static β of the electronic transition induced by the charge transfer.

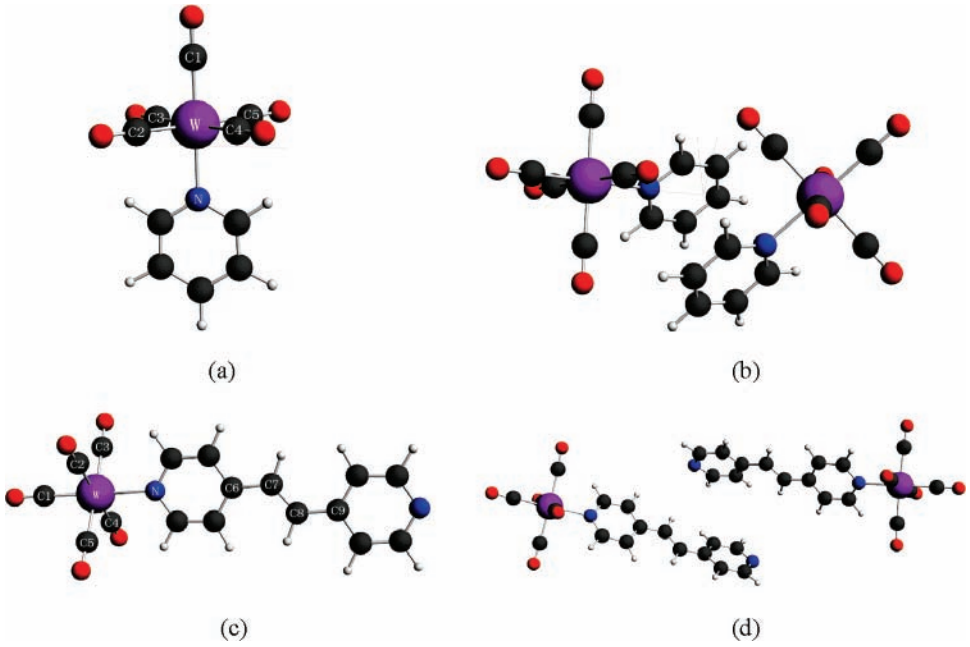

Figure 1. Molecular structures of model complexes (a) TPCP monomer; (b) TPCP dimer; (c) TPCB monomer; (d) TPCB dimer.

$$\beta_{\mathrm{CT}} \propto \frac{\Delta\mu_i M_i^2}{\Delta E_i^2} \tag{3}$$

where subscript i denotes the specified ith excited state. $\Delta\mu_i$ is the change of dipole moment after the ith excitation. M_i is the transition dipole moment and ΔE_i is the transition energy from the ground state to the ith excited state.

We adopted in this study the orbital decomposition scheme proposed by Hieringer and Baerends[12] in the analysis of the contribution of the orbital-pair transition to β. Assuming each excitation i could be decomposed into a series of orbital-pair transitions (a,b) with the different transition dipole moments $M_{(a,b)}$ and weight factors in percentage $c_{(a,b)}$. According to the orbital decomposition scheme, the contribution to β_{CT} of a specific orbital-pair transition is essentially meaningful and helpful rather than that of an individual excitation (i) in relating the electronic structure to β_{CT}. The contribution to β_{CT} of the specific orbital-pair transition (denoted by $\beta_{(a,b)}$, e.g., the contribution of HOMO to LUMO transition) in each excitation state (i) was summed up:

$$\beta_{(a,b)}^{\mathrm{CT}} = \sum_i^N \frac{\Delta u_i c_{(a,b)} M_{(a,b)}^2}{\Delta E_i^2} \tag{4}$$

where the summation is over all the calculated excited states (N) that possess the (a,b) orbital-pair transition. By this way, it could clearly show the relative contribution of the specific orbital-pair transition to β_{CT} to that of another orbital-pair transition. Equation 4 is used to evaluate the static first hyperpolarizability. The calculated static $\beta_{(a,b)}$ of the monomers of TPCP and TPCB with the dominant percentages and the relative ratios were listed in Tables 3 and 4, respectively.

All the calculations were performed on an IBM-JS21 server by the ADF program on release of 2006.01.

3. Results and Discussion

3.1. Electronic Structures and Electronic Excitation Spectra. *3.1.1. Monomer and Dimer of TPCP.* The orbital decomposition scheme and electronic structures are used in analyzing the origin of the electronic orbital transitions and their contributions to the first hyperpolarizability. Figure 2 shows the relevant frontier molecular orbital levels of TPCP monomer along with the constructed fragments of tungsten, carbonyl, and pyridine ligands. The highest three occupied orbitals, i.e., HOMO (belongs to a'' irreducible representation of the molecular point group, 19a''), HOMO-1 (belongs to a' irreducible representation of the molecular point group, 35a'), and HOMO-2 (34a') are typically in the d orbital character of tungsten atom with partial composition of typical metal−carbonyl-interacted orbitals (the lone pair electrons of carbonyls donate to the empty tungsten d orbitals and π back-donation from the d orbital to the empty π

TABLE 2: Dipole Moments (Debye), Dipole Polarizabilities (10^{-24} esu), and First Hyperpolarizabilities (10^{-30} esu) of Monomers and Dimers of TPCP and TPCB Complexes

complexes	μ	α_{static}	α_{1907}	β_{static}	β_{1907}	expt
TPCP-m	7.5	28.9	29.2	−11.0	−15.0	−4.4[a]
TPCP-d	5.7	56.5	56.9	−5.0	−6.5	−4.4[a]
TPCB-m	6.1	52.2	53.3	−66.0	−109.3	−7.0[b]
TPCB-d	4.2	102.2	104.2	−11.1	−21.5	−7.0[b]

[a] EFISH measured data in toluene solution at 1907 nm laser radiation, ref 9. [b] EFISH measured data in chloroform solution at 1907 nm laser radiation, ref 29.

TABLE 3: Orbital Decompositions of the Dominant Component β_{yyy} of TPCP Monomer (au), Supports That the Largest Orbital-Pair Contribution Has a Relative Ratio 100

(a,b)	β_{yyy}	ratio	dominant excitation contributions
(19a'',20a'')	−506.7	100	1A'(94%) + 2A'(4%)
(18a'',37a')	34.8	−6.9	12A'(17%) + 13A'(47%) + 25A'(9%) + 28A'(4%)
(18a'',23a'')	7.3	−1.4	12A'(8%) + 13A'(26%) + 25A'(25%) + 28A'(6%)

TABLE 4: Orbital Decompositions of the Dominant Component β_{xxx} of TPCB Monomer (au)

(a,b)	β_{xxx}	ratio	dominant excitation contribution
(73a,74a)	−8144.5	100	2A(94%) + 19A(4%)
(69a,74a)	2025.9	−24.9	2A(5%) + 19A(66%) + 28A(9%) + 29A(8%)
(72a,76a)	56.2	−0.7	9A(3%) + 10A(74%) + 13A(21%)

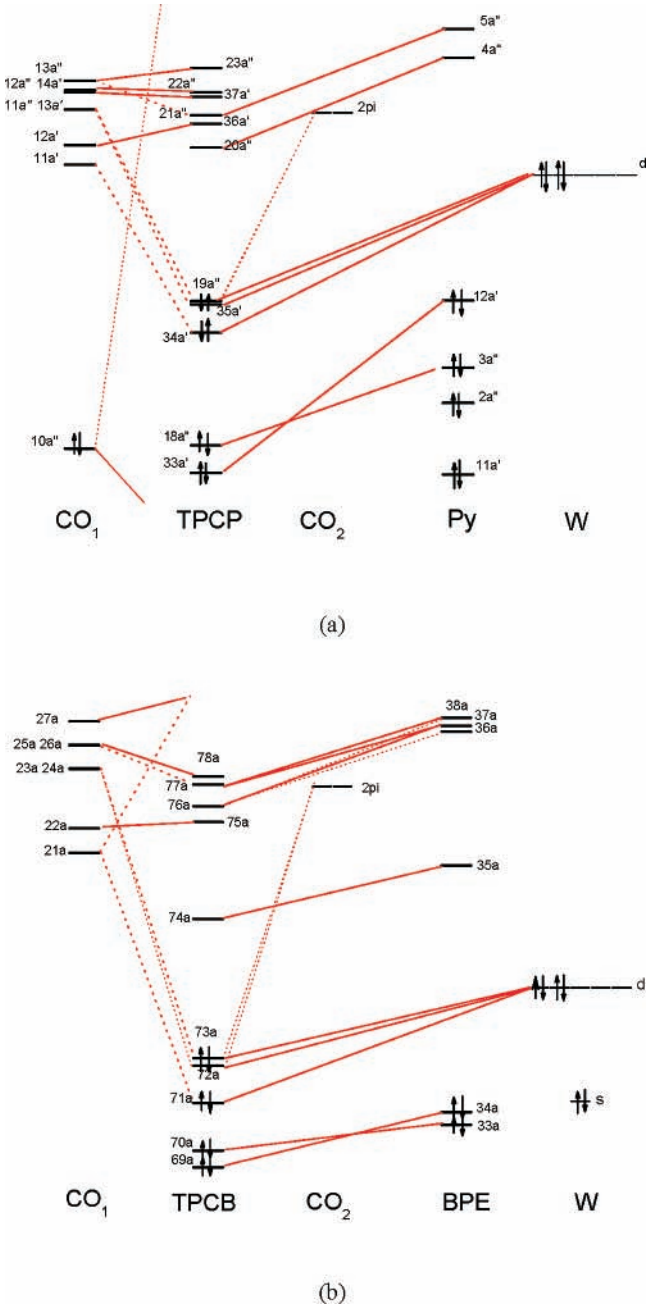

Figure 2. Frontier molecular orbital energy level diagrams of the monomers along with the constructed fragments (CO_1 denotes the four planar carbonyls and CO_2 for the other one. The solid lines show strong interactions and the dot lines for the weak ones). (a) TPCP monomer; (b) TPCB monomer.

orbitals of the four planar carbonyls). The next occupied orbital (18*a*″) is mainly characterized by the π-delocalization pyridine ligand. The low-lying unoccupied orbitals mainly belong to the ligand orbitals. LUMO (20*a*″) is characterized by the anti-π orbital of pyridine ligand, while the LUMO+1 (36*a*′) is entirely located on the four planar carbonyls (CO_1 in Figure 2).

The calculated electronic structure of the dimer TPCP presented the weak interaction between two constructed molecules. Figure 3a depicted the frontier orbitals of the dimer along with the two molecular fragments (m_1 and m_2). Most of the occupied frontier orbital are almost 2-fold generated (simply combines those of the single molecule), with about 0.2 eV energy lower than those of the molecular fragment. The LUMO (109*a*) and LUMO+1 however compose almost half LUMO of one molecule (m_1) and the half of the other (m_2) (LUMO: 0.46 m_1 + 0.50 m_2; LUMO+1: 0.48 m_1 + 0.46 m_2). The orbital energy of LUMO of dimer lowered about 0.15 eV with respect to that of the fragment, while for LUMO+1, it was about 0.1 eV higher. Because the LUMO and LUMO+1 of the dimer characterized by conjugated π^* orbital of the pyridine ligands, the intermolecular interaction acts mostly as the $\pi-\pi$ long-distance weak interaction between the two pyridines.

The electronic excitation spectrum measured by Cheng et al. showed that TPCP complex has a small d−L transition at 332 nm in toluene solution.[9] This transition was reported to be a poorly resolved excitation. Figure 4a showed the calculated excitation spectra of the monomer both in gas phase and in toluene solution. The low-energy excitations shifted to blue in solution for about 50 nm, while the high-energy peaks increased the intensities. Our results showed that the solvent effect exerts critical influence on the electronic excitation transition of the TPCP molecule in both energies and intensities. The d−L transition was found to be located at 388 nm in solution with a low calculated oscillator strength, $f = 0.003$, which corresponds is the poorly resolved peak in the measurement. The calculated result of Bruschi et al. was 401 nm, which was obtained in gas-phase calculation.

Within the spectrum region of 200−500 nm, more excitation transitions are presented in the excitation curve of the dimer (Figure 5a) because it includes the transitions of two constructed molecules. The results of dimer in solution assigned the λ_{d-L} located at 356 nm with a low oscillator strength ($f = 0.002$ in ADF calculation). The calculated value agrees well with the experimental data of 332 nm.

3.1.2. Monomer and Dimer of TPCB. TPCB monomer possesses a more extended π-delocalization ligand BPE than TPCP does. The electronic structure shows TPCB has a smaller HOMO−LUMO energy gap of 1.6 eV than TPCP does (2.3 eV). Figure 2b showed the frontier molecular orbitals along with the fragments of tungsten, carbonyl, and BPE ligands, which are similar to those of TPCP monomer. The highest three frontier occupied orbitals of HOMO (73*a*), HOMO-1 and HOMO-2 are typically the metal−carbonyl-based orbitals. The next two occupied lower-energy orbitals (70*a* and 69*a*) are characterized by the conjugated π orbital of BPE ligand. The LUMO (74*a*) is characterized by the empty anti-π orbital of BPE ligand, while the LUMO+1 is entirely located on the four carbonyls (CO_1).

The two molecules dimerized in such a configuration that *x*-axis is along the direction of two tungsten atoms *y* and *z* axes are perpendicular to the two BPE conjugated planes, respectively. The nearest distance between two molecules (m_1 and m_2) is 2.98 Å, much longer than the hydrogen bond length. This indicates the interaction between the two constructed molecules is very weak. The interaction of the virtual unoccupied orbitals of m_1 and m_2 did not happen in TPCB dimer. The electronic structure of TPCB dimer is mostly the combination of those of m_1 and m_2. To describe clearly in the following section, it is noted that the LUMO of the dimer (147*a*) mostly belongs to BPE of m_1 and LUMO+1 to that of m_2. The HOMO (146*a*) is mostly ascribed to m_1, while HOMO-1 is mostly ascribed to m_2 (Figure 3b).

Figure 4b showed the excitation spectra of TPCB monomer both in benzene solution and in gas phase. The low-energy excitations are once again found blue-shifted, while the high-energy excitations mostly reduced the intensities due to the solvent polarity. The replacement of Py by a more π-delocalized BPE ligand shifted low-energy excitation peaks to red by about 120 nm. The UV−vis spectrum measured by Pizzotti et al. obtained the $d_M - \pi^*_L$ (d−L) transition and $d_M - \pi^*_{CO}$ (d−

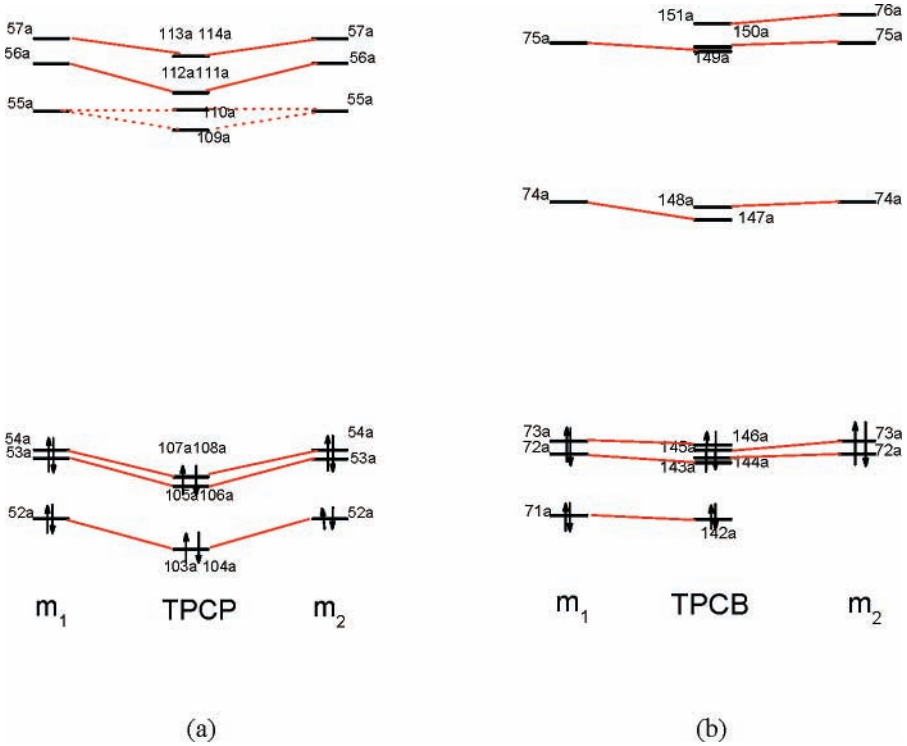

Figure 3. Frontier molecular orbital energy level diagrams of the dimers along with the constructed molecules (m_1 and m_2). (a) TPCP dimer; (b) TPCB dimer.

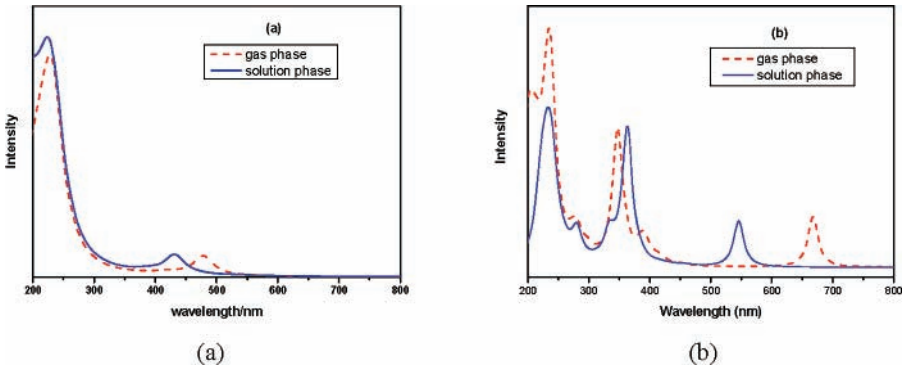

Figure 4. Simulated electronic excitation spectra in both the gas-phase (dash) and solution-phase (solid) of (a) TPCP and (b) TPCB monomer.

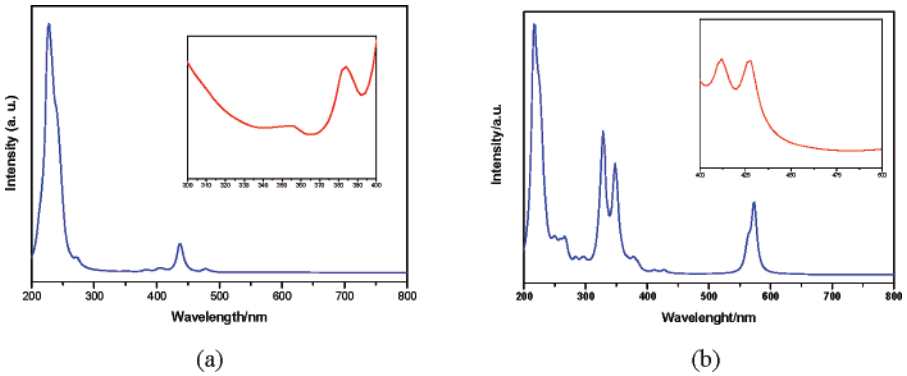

Figure 5. Simulated electronic excitation spectra in solution of (a) TPCP and (b) TPCB dimer.

CO) transition at 441and 403 nm, respectively.[29] The excitation results of the monomer showed that the d−L transition located at 487 nm with the calculated oscillator strength $f = 0.003$, while the d−CO transition located at 418 nm with $f = 0.008$. The previously reported calculate data in gas phase were 492 and 422 nm, respectively.[13] The results of monomer model in both cases overestimated the measurement.

The results of TPCB dimer in solution (Figure 5b) assigned the λ_{d-L} located at 437 nm with the oscillator strength $f = 0.002$, which mainly corresponds to the transition between the orbitals

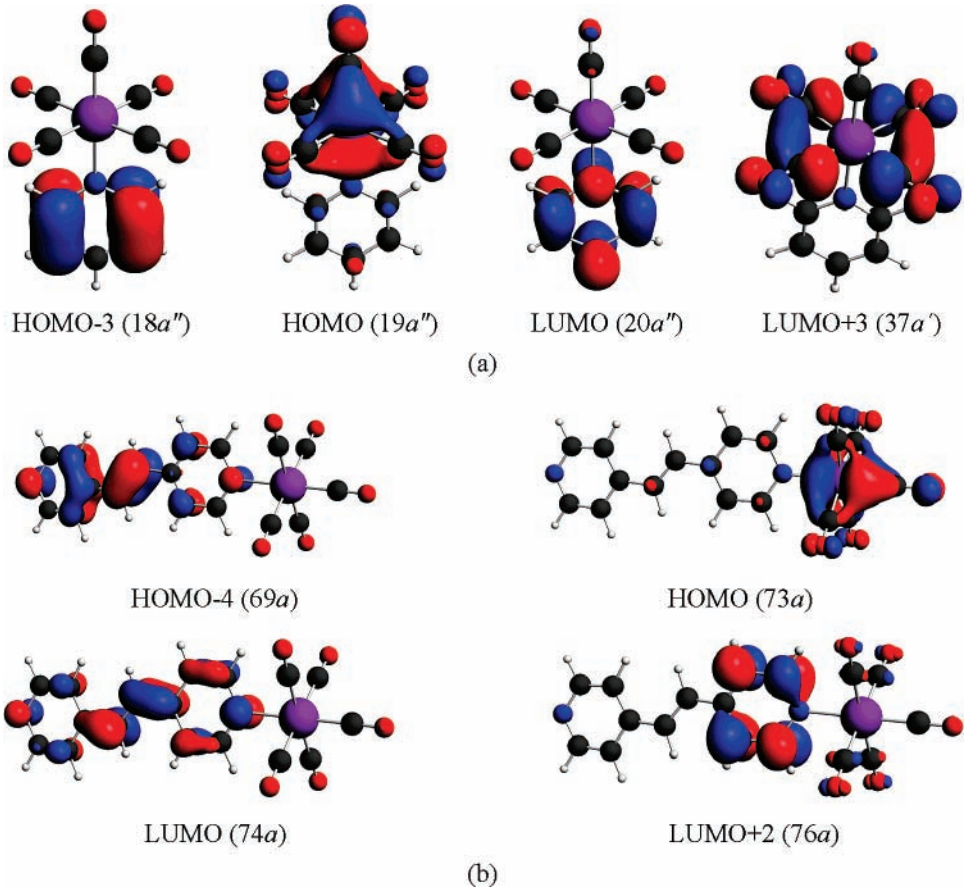

Figure 6. Molecular orbital contours involving the major charge transfers of (a) TPCP and (b) TPCB.

from 146*a* to 147*a* involving m_1. The calculated λ_{d-CO} located at 411 nm with the oscillator strength $f = 0.01$, which mainly corresponds to the transitions from 143*a* orbital to 149*a* orbital involving m_1 and from 144*a* to 150*a* involving m_2. The TDDFT results in this study agree well with the experimental data.

3.2. First Hyperpolarizability. *3.2.1. Monomer and Dimer of TPCP.* As a typical and simple metal−carbonyl aromatic complex, TPCP has been studied by various theoretical techniques before to understand the nature of the first hyperpolarizability. The charge transfer from metal to pyridine ligand has been ascribed to the major contribution to the β_{CT} in the literature.[13] The present study on TPCP by using the TDDFT method reproduced the conclusion of the earlier studies.

Table 2 lists both the calculated static and dynamic β_{vec} ($\approx \beta_y$) of the monomer in solution along with the dipole moments. The dynamic β_{vec} at 1907 nm was more than three times larger than the EFISH data. The result is apprehensible and is in concord with the previous studies[16] that DFT results usually overestimate β in magnitude. The static value of present study is larger in magnitude than the CPDFT gas-phase data reported by Bruschi et al.[13] This indicates that the solvent effect increases β of TPCP.

The calculations on TPCP dimer on the other side resulted in the significantly reduced β_y. The dynamic β_y value of -6.5×10^{-30} esu agrees with the experimental. The dipole moment (5.7 D) calculated by the dimer model was close to the measurement (6.0 D) as well. Although the results by the dimer approach were qualitatively satisfactory, β_{vec} was still 50% overestimated.

It is reasonable to assume that in most cases the environment effects including both the solvent effect and weak intermolecular interactions exert influence on the quantity of the first hyperpolarizability. With this idea in mind, we performed the orbital decomposition scheme only on the gas-phase monomers in the analysis process to address the intrinsic NLO nature of the molecules.

The results listed in Table 3 show that the dominant β_{yyy} component of β is ascribed mostly to the orbital-pair transition contribution of (19*a*″ 20*a*″), where 19*a*″ is the HOMO and 20*a*″ is the LUMO. This orbital-pair transition has been found to mainly come from the excitations of 1*A*′, the lowest energy excitation with medium intensity (the lower excitation contributions less than 2% are not listed in the second column of Tables 3 and 4). The second large contribution came from (18*a*″,37*a*′), where 18*a*″ is the HOMO-3 and 37*a*′ is the LUMO+3, and this contribution has the opposite sign of the largest one. The subsequent negative contribution to β_{yyy} is (18*a*″,23*a*′) transition. All other occupied to virtual orbital transitions are computed to have lower contribution to β_{yyy} less than 0.5% and are therefore not listed in Table 3.

The HOMO → LUMO transition is obviously characterized by MLCT ($d-\pi^*_L$), while the transitions of (18*a*″,37*a*′) and (18*a*″,23*a*′) are mainly originated to LLCT, both correspond mainly to the occupied π orbitals of the pyridine ligand to the empty π^* orbitals of the four planar carbonyls ($\pi_L-\pi^*_{CO}$). The LLCT contributions reduce the dominant MLCT contribution to β_{yyy} with a small relative ratio less than 9%.

3.2.2. Monomer and Dimer of TPCB. The first hyperpolarizability of TPCB has also been studied before by both SCI/SOS and DFT methods in gas phase.[13] Bruschi et al. stated by using sum-over-state (SOS) analysis that the intraligand charge transfer (ILCT) makes significant contribution to β_{CT}. We presented in this study the similar conclusion by using the orbital decomposition scheme, which is based on response theory.

The static β_{vec} ($\approx \beta_x$) computed by the monomer model in solution was -66×10^{-30} esu (Table 2), which is again larger than the earlier reported CPDFT data[13] in gas phase. The solvent effect increases β of TPCB. The dynamic β_{vec} on the other hand was more than fifteen times larger than that of the experimental data. The calculated dynamic β_{vec} by the dimer model greatly reduced to -21×10^{-30} esu. Considering the systematical error of the measurement and the XC approximation of the DFT method that we used, the dimer model in solution produced a satisfactory qualitative β of TPCB complex. It is also noteworthy that the dipole moment (4.2 D) by the dimer model in solution agrees well with the measurement (3.8 D).

The orbital decomposition scheme performed on the TPCB monomer in gas phase showed the orbital-pair transition that major contributed to β_{xxx} was (73*a*,74*a*), where 73*a* is the HOMO and 74*a* is the LUMO, which mainly came from the low-energy excitation of 2*A*. The second large contribution in magnitude came from (69*a*,74*a*) transition with a relative ratio of about 25% to the largest one. But its contribution has an opposite sign to that of the largest one. The third large contribution in magnitude that can also make an opposite contribution to β_{xxx} came from (72*a*,76*a*) orbital-pair transition. The molecular orbital analysis showed that (73*a*,74*a*) transition is basically MLCT (d$-\pi^*_L$), while (69*a*,74*a*) transition is ILCT inside BPE ligand from one pyridine ring to the other. The (72*a*,-76*a*) transition corresponds to MLCT (d$-\pi^*_{CO}$). Both the transitions of (69*a*,74*a*) and (72*a*,76*a*) made negative contribution to the magnitude of β_{xxx}. The ILCT contribution is about 25% in ratio of the MLCT contribution.

To conclude this section, the environment effects, particularly the intermolecular interaction, are important in the theoretical quantitative reproduction of the measured β. The orbital decomposition scheme based on the response theory clearly and usefully analyzes the NLO origin in terms of the linear optical parameters such as $\Delta\mu_i$, M_i, and ΔE_i (formula 4). Our results showed that the MLCT was the major charge transfer contributed to the first hyperpolarizability of both TPCP and TPCB chromophores (Figure 6). By substituting Py ligand with a more extended conjugated π-delocalization BPE ligand, the relative ratio of MLCT contribution to LLCT /ILCT contribution reduced and the β increased.

4. Conclusion

In this paper, we applied the high-level TDDFT method to calculate the electronic excitation spectra and the first hyperpolarizability of two typical tungsten−carbonyl arene chromophores, TPCP and TPCB. Both the solvent effect and weak intermolecular interactions have been taken into account in the computation and the calculated results have been significantly improved and are in satisfactory comparison with the experimental measurements, letting out the systematic experimental error and XC functional approximations.

We showed that the solvent effect exerts critical influence on the electronic excitations of TPCP and TPCB chromophores in both the excitation energies and intensities. The weak intermolecular interactions that existed in solution-phase EFISH measurement could be simulated by using the specified supermolecular models. We found that interaction effects, in particular the $\pi-\pi$ stacking interactions in TPCP and TPCB dimer, influence the calculated β values in quantity under the specified dimer configurations. It is necessary to consider the interaction effects in pursuing the satisfactory computing results in comparison with the experimental.

By using the new proposed orbital decomposition scheme by Baerends and his co-worker, we concluded that these two typical metal−carbonyl chromophores exhibited the dominant MLCT mechanism in NLO response. This useful scheme could easily clarify the essential orbital-pair transitions to the first hyperpolarizability in terms of the linear optical parameter obtained by the electronic excitation computations. We added supplementary formula 4 to implement the orbital decomposition analysis. It modified the crude TLM model and let it work in the study. By using this formula, the relative contribution of each orbital-pair transition to the other could be quantitatively obtained, and therefore the dominant charge-transfer pattern in NLO response could be easily assigned. This formula at present stage is available to the NLO-phores with one-dimensional charge transfers due to the finite-field scheme used in obtaining $\Delta\mu_i$.

The orbital decomposition scheme is practically convenient and computing economical compared to the traditional sum-over-state (SOS)[30] analysis scheme. As a result, most complicated systems could be affordable by this scheme. It is very promising to apply the scheme in the large-size complexes such as nanometer motifs, inorganic metal cluster complexes containing more than one TM atoms, and biological protein or DNA large molecules.

We ascribed the overestimations of TLM in estimating β of TPCP and TPCB chromophores to the missing states of LLCT and ILCT contributions. According to our analysis the LLCT contribution could reduce about 9% in total of β_{CT} in magnitude of TPCP and the larger percentage of reduction are found by ILCT contribution in TPCB case. The more extended conjugated delocalization ligand the complex has, the smaller energy gap would be (ΔE_g of TPCP is 2.3 eV and that of TPCB is 1.6 eV), which results in the reduced LLCT/ILCT transition energies. The LLCT/ILCT contributions to the β consequently increase because the transition energy is in inverse proportion to β_{CT} to the second power. The results strongly suggest that by adjusting the coordination conjugated ligand, the NLO mechanism of metal−carbonyl chromophores might be altered from MLCT dominant to LLCT/ILCT dominant. This is very interesting in designing and tailoring the tungsten−carbonyl complexes with specified NLO properties. More examples on this topic are currently in process in our group.

Acknowledgment. We acknowledge the financial support from the Ministry of Science and Technology of China for the projects 2004CB730605 and 2006DFA43020 and the National Science Foundation of China for projects 90203017 and 20573114.

References and Notes

(1) (a) Green, M. L. H.; Marder, S. R.; Thompson, M. E.; Bandy, J. A.; Bloor, D.; Kolingsky, P. V.; Jones, R. J. *Nature* **1987**, *330*, 360. (b) Long, N. J. *Angew. Chem., Int. Ed. Engl.* **1995**, *34*, 21. (c) Powell, C. E.; Humphery, M. G. *Coord. Chem. Rev.* **2004**, *248*, 725. (d) Gradinaru, J.; Forni, A.; Druta, V.; Tessore, F.; Zecchin, S.; Quici, S.; Garbalau, N. *Inorg. Chem.* **2007**, *46*, 884.

(2) (a) Shi, S.; Ji, W.; Tang, S. H. *J. Am. Chem. Soc.* **1994**, *116*, 3615. (b) Philip, R.; Kumar, R. G.; Mathur, P.; Ghose, S. *Opt. Commun.* **2000**, *178*, 469. (c) Maury, O.; Viau, L.; Senechal, K.; Corre, B.; Guegan, J. P.; Renouard, T.; Ledoux, I.; Zyss, J.; Le Bozec, H. *Chem.−Eur. J.* **2004**, *10*, 4454. (d) Coe, B. J. *Acc. Chem. Res.* **2006**, *39*, 383.

(3) (a) di Bella, S. *Chem. Soc. Rev.* **2001**, *30*, 355. (b) Coe, B. J.; Harris, J. A.; Brunschwig, B. S. *J. Phys. Chem.* **2002**, *106*, 897.

(4) (a) Bruce, D. W.; Thornton, A. *Mol. Cryst. Liq. Cryst.* **1993**, *231*, 253. (b) Robert, D.; Tessore, F.; Ugo, R.; Bruni, S.; Manfredi, A.; Quici, S. *Chem. Commun.* **2002**, 846. (c) Meyer-Friedrichsen, T.; Wong, T.; Prosenc, M. H.; Heck, J. *Eur. J. Inorg. Chem.* **2003**, 936.

(5) (a) Shin, Y. K.; Brunschwig, B. S.; Creutz, C.; Satin, N. *J. Phys. Chem.* **1996**, *100*, 8157. (b) Coe, B. J.; Jones, L. A.; Harris, J. A.; Brunschwig, B. S.; Asselberghs, I.; Clays, K.; Garin, J.; Orduna, J. *J. Am. Chem. Soc.* **2004**, *126*, 3880.

(6) (a) Wu, K. C.; Sa, R. J.; Lin, C. S. *New J. Chem.* **2005**, *29*, 362. (b) Chen, X. H.; Wu, K. C.; Snijders J. G.; Lin, C. S. *Inorg. Chem.* **2003**, *42*, 532. (c) Wu, K. C.; Lin, P.; Wu, X. T.; Chen, L. *Laser Chem.* **2000**, *18*, 193.

(7) (a) Pizzotti, M.; Ugo, Dragonetti, R. C.; Annoni, E.; Demartin, F.; Mussin, P. *Organometallics* **2003**, *22*, 4001. (b) Garcia, M. H.; Royer, S.; Robalo, M. P.; Dias, A. R.; Tranchier, J. P.; Chavignon, R.; Prim, D.; Auffrant, A.; Rose-Munch, F.; Rose, E.; Vaissermann, J.; Persoons, A.; Asselberghs, I. *Eur. J. Inorg. Chem.* **2003**, 3895.

(8) Lamère, J. F.; Sasaki, I.; Lacroix, P. G.; Nakatani, K. *New J. Chem.* **2006**, *30*, 921.

(9) (a) Cheng. L. T.; Tam, W.; Eaton, D. F. *Organometallics* **1990**, *9*, 2856. (b) Cheng. L. T.; Tam, W.; Meredith, G. R. *Mol. Cryst. Liq. Cryst.* **1990**, *189*, 137.

(10) (a) Ricciardi, G.; Rosa, A.; van Gisbergen, S. J. A.; Baerends, E. J. *J. Phys. Chem.* **2000**, *104*, 635. (b) Karton, A.; Iron, M. A.; van der Boom, M. E.; Martin, J. M. L. *J. Phys. Chem.* **2005**, *109*, 5454.

(11) (a) Senechal-David, K.; Hemeryck, A.; Tancrez, N.; Toupet, L.; Williams, J. A. G.; Ledoux, I.; Zyss, J.; Boucekkine, A.; Guegan, J. P.; Le Bozec, H.; Maury O. *J. Am. Chem. Soc.* **2006**, *28*, 12243. (b) Romaniello, P.; Lelj, F. *J. Mol. Struct. (THEOCHEM)* **2003**, *636*, 23.

(12) Hieringer, W.; Baerends, E. J. *J. Phys. Chem. A* **2006**, *110*, 1014.

(13) (a) Bruschi, M.; Fantucci, P.; Pizzotti, M. *J. Phys. Chem. A* **2005**, *109*, 9637. (b) Bruschi, M.; Fantucci, P.; Pizzotti, M.; Rovizzi, C. *J. Mol. Catal. A* **2003**, *204*, 793.

(14) Oudar, J. L. *J. Chem. Phys.* **1977**, *67*, 446.

(15) (a) Inerbaev, T. M.; Belosludov, R. V.; Mizuseki, H.; Takahashi, M.; Kawazoe, Y. *J. Chem. Theory Comput.* **2006**, *2*, 1325. (b) Cundari, T. R.; Kurtz, H. A.; Zhou, T. *J. Phys. Chem. A* **2000**, *104*, 4711. (c) Sainudeen, Z.; Ray, P. C. *J. Phys. Chem. A* **2005**, *109*, 9095.

(16) (a) Cundari, T. R.; Kurtz, H. A.; Zhou, T. *J. Chem. Inf. Comput. Sci.* **2001**, *41*, 38. (b) Wu, K. C.; Snijders, J. G.; Lin, C. S. *J. Phys. Chem. B* **2002**, *106*, 8954. (c) Skwara, B.; Bartkowiak, W.; Zawada, A.; Gora, R. W.; Leszczynski, J. *Chem. Phys. Lett.* **2007**, *436*, 116. (d) *J. Chem. Phys.* **2007**, *126*, 154316.

(17) (a) Champagne, B.; Perpete, E. A.; Jacquemin, D.; van Gisbergen, S. J. A.; Baerends, E. J.; Soubra-Ghaoui, C.; Robins, K. A.; Kirtman, B. *J. Phys. Chem. A* **2000**, *104*, 4755. (b) Champagne, B.; Perpete, E. A.; van Gisbergen, S. J. A.; Baerends, E. J.; Snijders, J. G.; Soubra-Ghaoui, C.; Robins, K. A.; Kirtman, B. *J. Chem. Phys.* **1998**, *109*, 10489. (c) van Gisbergen, S. J. A.; Schipper, P. R. T.; Gritsenko, O. V.; Baerends, E. J.; Snijders, J. G.; Champagne, B.; Kirtman, B. *Phys. Rev. Lett.* **1999**, *83*, 694.

(18) (a) Klamt, A. *J. Phys. Chem.* **1995**, *99*, 2224. (b) Klamt, A.; Jones, V. *J. Chem. Phys.* **1996**, *105*, 9972.

(19) Klamt, A.; Schüürmann, G. *J. Chem. Soc.: Perkin Tans.* **1993**, *2*, 799.

(20) Klement, U. *Z. Kristall.* **1993**, *208*, 111.

(21) (a) Gaus, P. L.; Boncella, J. M.; Rosengren, K. S.; Funk, M. O. *Inorg. Chem.* **1982**, *21*, 2174. (b) Zulu, M. M.; Less, A. J. *Inorg. Chem.* **1988**, *27*, 1139. (c) Pizzotti, M.; Ugo, R.; Roberto, D.; Bruni, S. *Organometallics* **2002**, *21*, 5830.

(22) (a) Ceperly, D. M.; Alder, B. J. *Phys. Rev. Lett.* **1980**, *45*, 566. (b) Vosko, S. H.; Wilk, L.; Nusair, M. *Can. J. Phys.* **1980**, *58*, 1200.

(23) (a) Becke, A. D. *Phys. Rev. A* **1988**, *38*, 3098. (b) Perdew, J. P. *Phys. Rev. B* **198**, *33*, 8822.

(24) (a) van Lenthe, E.; Baerends, E. J.; Snijders, J. G. *J. Chem. Phys.* **1993**, *99*, 4597. (b) van Lenthe, E.; Baerends, E. J.; Snijders, J. G. *J. Chem. Phys.* **1996**, *105*, 6505.

(25) van Gisbergen, S. J. A.; Snijders, J. G.; Baerends, E. J. *J. Chem. Phys.* **1998**, *109*, 10644.

(26) te Velde, G.; Bickelhaupt, F. M.; Baerends, E. J.; Fonseca-Guerra, C.; van Gisbergen, S. J. A.; Snijders, J. G.; Ziegler, T. *J. Comput. Chem.* **2001**, *22*, 931.

(27) Gruning, M.; Gritsenko, O. V.; van Gisbergen, S. J. A.; Baerends, E. J. *J. Chem. Phys.* **2001**, *114*, 652.

(28) van Leeuwen, R.; Baerends, E. J. *Phys. Rev. A* **1994**, *49*, 2421.

(29) Pizzotti, M.; Ugo, R.; Roberto, D.; Bruni, S. *Organometallics* **2002**, *21*, 5830

(30) Ward, J. F. *Rev. Mod. Phys.* **1965**, *37*, 1.